

Virus Assembly Pathways: Straying Away but Not Too Far

Kevin Bond, Irina B. Tsvetkova, Joseph Che-Yen Wang,* Martin F. Jarrold,*
and Bogdan Dragnea*

Non-enveloped RNA viruses pervade all domains of life. In a cell, they co-assemble from viral RNA and capsid proteins. Virus-like particles can form in vitro where virtually any non-cognate polyanionic cargo can be packaged. How only viral RNA gets selected for packaging in vivo, in presence of myriad other polyanionic species, has been a puzzle. Through a combination of charge detection mass spectrometry and cryo-electron microscopy, it is determined that co-assembling brome mosaic virus (BMV) coat proteins and nucleic acid oligomers results in capsid structures and stoichiometries that differ from the icosahedral virion. These previously unknown shell structures are strained and less stable than the native one. However, they contain large native structure fragments that can be recycled to form BMV virions, should a viral genome become available. The existence of such structures suggest the possibility of a previously unknown regulatory pathway for the packaging process inside cells.

viruses, the CPs can self-assemble in vitro around a variety of non-genomic cargo,^[6] forming shells that can be structurally identical to those of the wild type (wt) virus. However, wt virus assembly inside the heterogeneous, crowded environment of a host cell cytoplasm surprisingly leads to the large majority of virions being laden with genomic RNA.^[7]

The reason for non-specific encapsulation in vitro is relatively well understood.^[5,8] The main driving force behind assembly at physiological ionic strengths are electrostatic interactions.^[9] By comparison, the rate of empty capsids assembly, which can occur when electrostatic interactions are screened, is several orders of magnitude slower than co-assembly of coat proteins in presence of polyanionic species.^[10] The question is then, how does

a virus avoid production of virus-like particles that encapsulate many of the smaller, non-viral, transient RNAs and other polyions occurring in the cytoplasm? In attempting to answer this long-standing question we have studied the nature of chimeras which assemble out of small ssDNA oligonucleotides and viral coat protein. Cryo-electron microscopy (cryo-EM) and charge detection mass spectrometry (CDMS) analysis of in vitro assembly products suggest that CP shells do readily form around multiple oligonucleotides. However, these shells have specific, strained structures which easily split into large fragments. These may provide intermediates for correct, fast virion growth when cognate RNA, containing appropriate packaging signals becomes available.^[11–13]

1. Introduction

Small nonenveloped icosahedral positive-sense RNA viruses infect all domains of life. This broad class encompasses important pathogens including poliovirus, rhinovirus (the cause of common cold), and aphthovirus (the cause of foot and mouth disease). A deeper understanding of their assembly mechanisms could lead to design principles for novel antivirals,^[1,2] and facilitate the development of a range of useful viromimetic nanoparticles.^[3,4] The viral genome plays an active role in assembly.^[5] It recruits coat proteins (CPs) that ultimately package the RNA spontaneously by self-organizing into a symmetric, protective shell. For a few single stranded (ssRNA)


2. Results and Discussion

In this work, virus-like particles (VLPs) were formed by mixing purified coat proteins of the brome mosaic virus (BMV) with two types of ssDNA oligonucleotides, both 52 nucleotides long. The two oligonucleotide fragments had different tertiary structures: the first one, hereafter called oligoB, originated from the BMV RNA genome sequence that interacts with the BMV CP N-terminal arm.^[14,15] The second oligomer was a linear polyA polymer with no tertiary structure (see Figures S1 and S2, Supporting Information for assembly conditions, biochemical characterization, and transmission electron microscopy (TEM) characterization).

To determine the masses of the VLPs formed, we employed charge detection mass spectrometry (CDMS). CDMS measures

Dr. K. Bond, Dr. I. B. Tsvetkova, Prof. M. F. Jarrold, Prof. B. Dragnea
Department of Chemistry
Indiana University
Bloomington, IN 47405, USA
E-mail: mfj@indiana.edu; dragnea@indiana.edu

Prof. J. C.-Y. Wang^[†]
Electron Microscopy Center
Indiana University
Bloomington, IN 47405, USA
E-mail: joewang@psu.edu

 The ORCID identification number(s) for the author(s) of this article can be found under <https://doi.org/10.1002/smll.202004475>.

^[†]Present address: Department of Microbiology and Immunology, Pennsylvania State University College of Medicine, Hershey, PA 17033, USA

DOI: 10.1002/smll.202004475

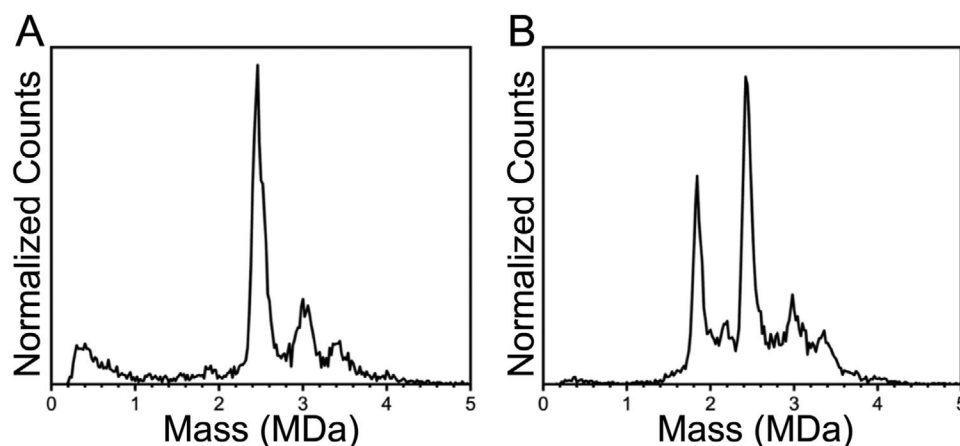


Figure 1. CDMS spectra of BMV CP assembled around A) polyA, and B) oligoB. The samples were prepared by mixing BMV CP to oligo at the molar ratio 15:1 at 4 °C and low ionic strength. The data was collected 1 week after the assembly reaction was initiated. In the CDMS spectrum of CP assembled on polyA, there are three major peaks at 2.5, 3, and 3.4 MDa. BMV CP assembled with oligoB shows an additional peak at 1.9 MDa.

the mass to charge ratio and the charge for each ion simultaneously, which allows for the direct determination of the mass at a single particle level; thus, it enables analysis of a heterogeneous sample.^[16,17] Each oligomer sample was measured at least twice: immediately after mixing the assembly reaction and two weeks after mixing (Figures S4 and S5, Supporting Information).

In agreement with previous work,^[18–20] size histograms obtained from negative stain TEM (Figure S1, Supporting Information) indicate that the dominant diameters for both types of cargo correspond to shells that are smaller than the native $T = 3$ capsid. Such smaller particles have been observed before and have been often associated with pseudo- $T = 2$ shells. The mass of an empty $T = 2$ particle is ≈ 2.44 MDa. The *N-termini* of BMV coat protein consist of highly basic flexible arginine rich motif (ARM) carrying nine positive charges which interacts with viral RNA.^[21] Assuming a charge ratio of ≥ 1 nucleotide/coat protein ARM,^[22] one would expect the most probable particle mass to be at least ≈ 2.75 MDa. Intriguingly, the CDMS mass spectra (Figure 1) for both reactions deviate from this expectation. Thus, both BMV-VLP/polyA and BMV-VLP/oligoB have the sharpest and most prominent mass peak located at $\approx 2.5 \pm 0.1$ MDa, well below the pseudo- $T = 2$ expected mass. The distribution does extend to higher masses, with two other minor peaks at mass of 3 MDa and 3.4 MDa. BMV-VLP/oligoB showed an additional major mass peak at around 1.9 MDa (Figure 1B). These multiple, distinctly separated, mass peaks account for roughly 70% of the total number of ions, leaving about 30% of the ions located in between the main peaks. Those are presumably associated with incomplete or malformed particles.

These discrepancies between expected and measured masses warrant further inspection. Let us assume first that the closed shells observed in TEM and the most prominent peaks correspond to same stable species in solution. Taking an Occam's razor approach, let us further assume the structures of closed shells obey the Caspar–Klug rules of quasi-equivalence. In this case, considering 16 kDa molecular weight for each polyA and oligoB, the mass peaks at 2.5 MDa and 3.0 MDa observed in both

VLPs could correspond to a cage with pseudo- $T = 2$ symmetry (60 dimers of BMV CP) packaging 6 and 33 oligomers, respectively. However, the total net charge on the luminal interface of a pseudo- $T = 2$ capsid is ≈ 1080 positive charges.^[21] Each oligo provides 52 negative charges. Then, the 6 oligomers (312 charges) in the case of the 2.5 MDa peak should be far too little to stabilize a closed capsid at low ionic strength.

In the case of the 3.0 MDa peak, 33 oligoes carry 1716 charges, and provide ≈ 1.6 nucleotide/coat protein ARM charge ratio. This ratio is higher than expected for short oligoes but comparable with the overcharging observed in the case of many single-stranded RNA viruses.^[8]

We now turn our attention towards the 3.4 MDa peak. An empty $T = 3$ capsid would have a mass of 3.65 MDa. Since there is no significant presence of ions above 3.4 MDa, we do not believe that $T = 3$ capsids could be present, empty or not. For a pseudo- $T = 2$ capsid, the 3.4 MDa VLP would correspond to a particle packaging 60 oligos (3120 charges) which is far too many charges to make a stable construct.

Further, the mass peak at 1.9 MDa observed for BMV-VLP/oligoB (Figure 1B) has too small a mass even for an empty $T = 2$ particle. If we assume a closed shell with $T = 1$ symmetry (30 dimers of BMV CP, 1.22 MDa) the amount of packaged oligoes is 43. That is a cargo charge ≈ 4 times the luminal interface charge, which is very unlikely. Moreover, there were no visually detectable $T = 1$ sized particle observed in the negative stain TEM image (Figure S1B, Supporting Information).

To sum up, at this point of our analysis, the 3.0 MDa peak is the only one that could correspond to a closed shell with pseudo- $T = 2$ symmetry. The rest of the prominent assembly products must be non-icosahedral. To further investigate this possibility, structural analysis of the assemblies was performed by cryo-EM with no imposed symmetry applied during 3D reconstructions.

Inspection of assembly results by cryo-EM supports the picture emerging from TEM data: two distinct BMV-VLP sizes (22 and 25 nm) can be observed in the cryo-EM micrographs (Figure 2). The smaller VLPs, roughly similar in size with a pseudo- $T = 2$ particle, are the dominant population

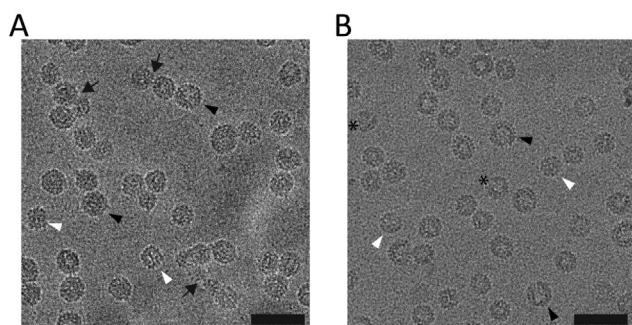


Figure 2. Cryo-EM micrographs with representative assembly results for A) BMV-VLP/poly-A and B) BMV-VLP/oligoB. In BMV-VLP/poly-A, some individual particles show faceted morphology (white arrowhead), while a subset of particles with larger diameter appear to be more circular (black arrowhead). Some malformed complexes seem to share nucleic acid (black arrow). In BMV-VLP/oligoB, both small (white arrowhead) and large (black arrowhead) particles are observed. However, the interior seems to have less density compared to BMV-VLP/polyA. Some incomplete or aberrant particles were also observed (asterisk). Scale bar, 50 nm.

(Figure 2, white arrowhead). Interestingly, these smaller particles appear to have more angular surface profile as compared to the smooth and circular morphology of the larger particles. As in the negative stain images, no $T = 1$ sized particles were observed. Aberrant and incomplete particles have been observed, in smaller measure, in both preparations (Figure 2). These particles, which show low internal density or have a broken outer surface, could correspond to the population of particles that have been previously reported to be sensitive to RNase digestion.^[20]

PolyA appears to promote formation of multiplsets that were previously only seen when assembling VLPs using cargo longer than the native genome^[20,23,24] (Figure 2A, arrow). In this context, we note that the persistence length of polyA (the length at which a polymer will behave as a rigid rod) is 40 nm,^[25] which is longer than the 52-nt polyA used in our experiments

(16 nm). Based on this observation, it is reasonable to expect that folding and compression of the nucleic acid into a spherical shape would be associated with a high free energy penalty for this cargo. Instead, the nucleo-protein complexes would be more likely to take a non-spherical shape, as in the "beads on a string" formations. However, there are clearly other, more stable solutions to this problem, which apparently include closed cages. What are their structures?

To characterize the structural organization and the uniformity of the particles, we applied unbiased 2D classification on both VLP images. Previously, 2D classification was used to identify icosahedral capsids that were distorted due to a small molecule.^[26] It was also demonstrated that 2D classification can clearly identify particles that are incomplete or overgrown.^[27,28] In fact, one of the most powerful features of the 2D class averaging is to increase the signal-to-noise ratio by averaging away some dissimilarities inside a class, allowing one to visualize the actual structural elements, without bias from symmetry operations.

Intriguingly, in both sets of VLPs, we observed that a large fraction of particles exhibited fourfold rotational symmetry as evidenced in the class averages by 4 or 8 similar densities at the capsid surface and a square-like outline (Figure 3B, e.g. second panel, and Figure S6, Supporting Information). These particles have an apparent diameter of ≈ 22 nm—the same diameter as had been previously associated with pseudo- $T = 2$ symmetry particle.^[18,19,29] In addition to fourfold symmetry, we also identified threefold, fivefold, and sixfold symmetry elements. These symmetry elements indicate a novel structural organization, other than icosahedral. This structure was not identified in any of the previous *in vivo* or *in vitro* assembly experiments with coat proteins of icosahedral viruses. In addition to the 22-nm diameter VLP, a small fraction of class averages had a larger diameter and presents a more circular surface feature. These class averages, corresponding to a slightly elliptical particle, had an average diameter of 26 nm, which is smaller than the 28 nm of the native BMV $T = 3$ shell. Symmetrical elements

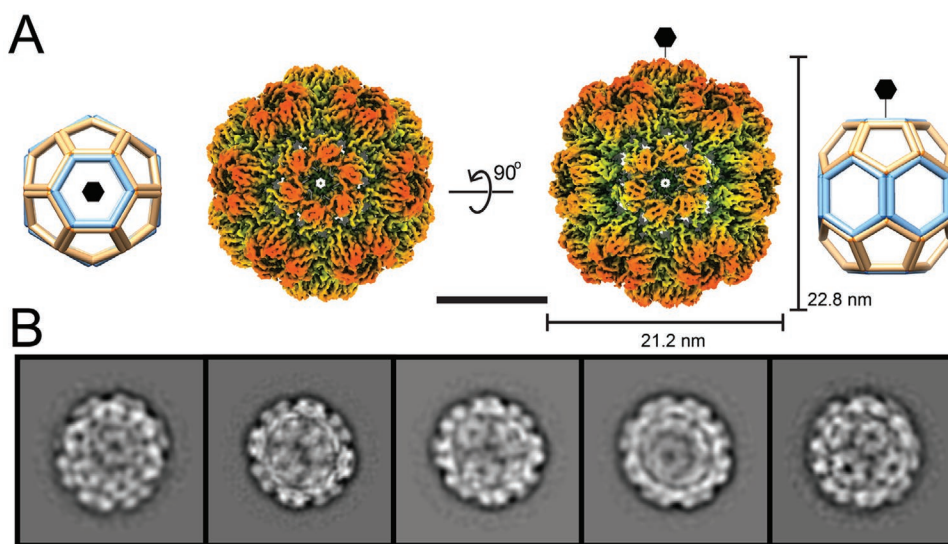


Figure 3. Cryo-EM structure of the H8 assembly. A) Isosurface representations of H8 rendered at different angles and the related views from symmetrical cage. The sixfold symmetry axis is marked. Scale bar is 10 nm. B) Selected reference-free 2D class averages show different orientations of the particle.

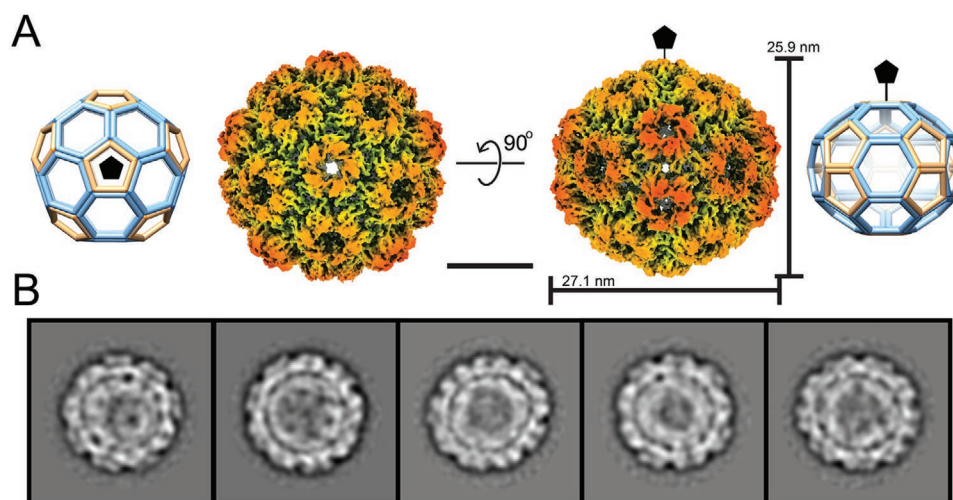


Figure 4. Cryo-EM structure of the H15 assembly. A) Isosurface representations of H15 rendered at different angles and the related views from symmetrical cage. The fivefold symmetry axis is marked. B) Selected reference-free 2D class averages show different orientations of the particle. Scale bar is 10 nm.

like threefold, fivefold, and sixfold organization can be clearly seen in the 2D classes.

To avoid model bias from any known structures, we separated small and large particles and built the initial model using the stochastic gradient descent algorithm implemented in Relion 3.0 without applying any symmetry.^[30] The resulting 3D models were further refined asymmetrically (Supporting Information). Once the structures converged, they were examined for potential symmetry which could be applied to boost the signal. The final 3D reconstructions for small 22-nm VLPs were refined to 3.6 Å for oligoB and 5.3 Å for polyA using D6 symmetry (Figure 3 and Figure S8, Supporting Information). Reconstructions for the two cargoes converged to the same structure, hereby called H8. Data presented in the manuscript is from H8 encapsulating oligoB, while data from H8 encapsulating polyA can be found in the Supporting Information. The larger (≈ 26 nm) VLPs were refined to 4.3 Å for oligoB (hereby called H15) and 7.2 Å for polyA (Figure 4 and Figure S8, Supporting Information, respectively).

Structure orientations of the H8 particle exhibit easily recognizable, cyclic sixfold-symmetric top and bottom views, as well as elliptical twofold-symmetric side views (Figure 3A). Thus, the H8 structure corresponds to a D6 hexagonal barrel containing 12 pentameric and eight hexameric capsomers (hence the name) in an arrangement of one hexameric capsomer at the opposing polar ends (top and bottom views along sixfold symmetry axis), followed by six pentameric capsomers at each side, and finally joined by a central belt of six hexameric capsomers. From the side view, the H8 particle measures 21.2 nm \times 22.8 nm. The top view exhibits six equally spaced pentameric capsomers arranged around a hexameric capsomer at the center with a common rotation axis (Figure 3A, left). The fourfold element, as seen in the 2D class averages, is not truly a fourfold axis, but rather a projection representation of four capsomers arranged according two orthogonal mirror axes. This explains the four circular ring densities that can be seen Figure 3B. A cage diagram representing the overall structure is provided in

Figure 3A. To the best of our knowledge, this is the first time experimental evidence has been found for capsid proteins of an icosahedral virus organized in this spatial configuration. The only other known biological structure with similar symmetry was observed in the in vitro packing of clathrin triskelions.^[31,32] The fact that the 3D reconstruction of the D6 barrel clathrin coat was done in the early days of cryo-EM of frozen hydrated specimens attests to the rigidity of this structure.^[31]

We now turn our attention to the large particle, H15, which also exhibits an unusual packing, Figure 4. Despite apparent size similarity, the unsupervised 2D class averages resulted in structural features that are starkly different from $T = 3$ particles. Thus, H15 contains 12 pentameric and 15 hexameric capsomers: two pentameric capsomers, one at each pole of the C5 rotational axis, surrounded by five hexameric capsomers; the central region contains a belt made of five pairs of adjacent pentameric capsomers, each pair being separated by a hexamer (Figure 4A). One notes nine “inverted cup-like” densities protruding at the capsid surface in most of the orientations, Figure 4B and Figure S6, Supporting Information. Furthermore, while for the first two selected 2D class averages in Figure 4B capsomer organization pattern dominates contrast, in the later three classes one can easily observe an additional layer of density underneath the capsid surface, while the capsomers remain aligned. This internal density is likely due to the N-terminal arm in association with the encapsidated oligos.

Having found the structures of the most abundant complete particles in the cryo-EM preparations, we can now attempt to assign them to the observed CDMS peaks. The H8 particle consists of 108 proteins, for a total protein mass of 2.19 MDa. To reach a total mass of 2.51 MDa, 20 encapsulated oligomers would be needed. This amount of nucleic acid provides almost exactly (1.07 ratio) the charge required to neutralize the positively charged residues of the luminal interface.

The H15 particle consists of 150 proteins. The protein cage alone has a mass of 3.05 MDa. This mass is observed in CDMS. However, to neutralize all the N-terminal arms at the luminal

interface, the cage should encapsulate ≈ 26 oligomers. The total mass predicted from encapsulating those is 3.46 MDa, which is close to the CDMS peak at 3.4 MDa.

There is one prominent peak in the oligoB assembly that could not be directly assigned to any of the observed closed-cage cryo-EM structures: the 1.9 MDa peak. We infer this peak must correspond to a partial nucleo-protein complex. Indeed, an abundance of broken particles can be seen in cryo-EM images of oligoB VLPs, Figure 2. We will return to the discussion of this intermediate shortly, when we will address the issue of elastic stress in the closed-cage structures H8 and H15.

The analysis so far leads to the conclusion that *in vitro*, short oligonucleotides promote assembly of BMV coat proteins into (metastable) particles with somewhat smaller protein shells than those of the wild-type BMV. Surprisingly, these shells are also of lower symmetry than the native BMV structure even when the size is comparable, as in the case of H15. Might there be a biological advantage behind these new observations of lower symmetry metastable particles?

Previous theoretical studies dealt mainly with simulation conditions resulting in high symmetry shells and their intermediates,^[33–37] but recently, Wagner and Zandi proposed a minimal model which demonstrates how lower symmetry shells can grow by irreversible addition of identical, deformable subunits.^[38] In their model, growth is guided by internal elastic stresses born out of mechanical properties of the subunits and geometric frustration. In a subsequent paper,^[39] they found striking similarities between the minimum free energy structure diagram and the diagram obtained via irreversible growth. These new simulations recapitulate the formation of high-symmetry shells as well as of lower symmetry ones. The crucial ingredients are the preferred (intrinsic) curvature and the mechanical parameters (stretching and bending moduli) of the subunits. Pentamers create more local curvature than hexamers. Thus, the addition of capsomers becomes selective depending on which capsomer creates more global stress when binding at the growing edge. For instance, at small intrinsic radii of curvature, adjacent hexamers would be disfavored. This is the case for the H8 particle, for instance, with its D6 barrel structure, which was found at the lowest end of the intrinsic radii range investigated by Wagner and Zandi.^[38] This is interesting because the intrinsic radius for the D6 barrel structure was predicted to be ≈ 1.5 times less than the intrinsic radius that led to the native structure. As empty BMV capsids having a structure identical to that of the wt BMV do assemble in absence of RNA, then the intrinsic radius of the RNA-free CP subunit should be ≈ 14 nm. Therefore, binding of small oligos to the CP reduces the apparent intrinsic radius of the assembly subunit (to about 10 nm, per Wagner and Zandi's calculations). Part of the binding energy in the pentamer-rich H8 and H15 particles is thus consumed to induce curvature, which presumably reduces the gain in free energy at assembly—the observed structures are pre-stressed and metastable. Pre-stress explains why they are rigid enough to be imaged with good resolution. As stress is distributed anisotropically,^[40] regions of high stress are more likely to yield, and the fragmentation pattern is deterministic, which is why we might see a sharp peak at 1.9 MDa (instead of a broad distribution). None of the observed closed shells correspond to this mass. We tentatively assign the

1.9 MDa peak to a fragment of the H15 particle because its presence is anticorrelated with that of H15 (see Figure S5, Supporting Information). The complement fragment at 1.5 MDa which is missing from mass histograms. This fragment might be more unstable. It has been suggested that the formation and meta-stability of partially assembled shells are dominated by an effective line-tension.^[41] Since the elastic stresses that develop upon assembly are relieved at the growing edge, the line tension depends on the stoichiometry and geometry of the partial shell—some fragments are more stable than others. The structure of the 1.9 MDa particle remains unclear at this point. Attempts at reconstruction were unsuccessful, probably because deterministic fragmentation does not necessarily imply that the resulting structures are static.^[41]

In support of the idea of metastability of lower-symmetry particles, we note that Tresset and collaborators have recently observed by Monte Carlo simulations that the cost of elastic energy of a non-symmetric shell assembling around a genomic template is so high that the partial capsids formed under non-equilibrium conditions will eventually repair themselves and form equilibrated symmetric structures.^[42]

In the context of fragmentation products of the metastable H8 and H15 particles, we note that the top or bottom halves of H15 have a structure that is very similar to that of a $T = 3$ icosahedral particle. Therefore, the angle between the pentameric–hexameric capsomers and hexameric–hexameric capsomers are similar with those encountered in wt BMV (Figure S12, Supporting Information). Actually, the pentamer–hexamer angles in H8 are also similar to those found in BMV. However, the angles of pentameric–pentameric or hexameric–hexameric capsomers (in H15) are smaller, thus contributing to form a squeezed conformation (in H15). The potential implication is that we are dealing with pre-stressed structures, with stresses concentrated at particular locations according to symmetry and interspersed among fragments of similar structure with the wt BMV. Therefore, because the 12 fivefold disclinations of a closed cage repel each other, structures with adjacent disclinations as the ones observed should exhibit locally higher elastic stress energy.^[43] Due to this excess elastic energy, subviral shells might be less stable, more prone to disassembly and kinetic bottleneck effects during growth than the wt BMV shell. The subviral particles can be observed because some of this excess energy is balanced by the nucleic acid cargo binding, which stabilizes the particles. However, so far such subviral empty cages have not been observed for BMV in the absence of nucleic acid, while empty $T = 3$ BMV cages form readily *in vitro*. This suggests that the subviral particles are metastable with respect to wtBMV. Let us assume for a moment that such a metastable particle would start forming around non-cognate small RNAs in the cell during infection. Then, if the particle fragmented, or if its growth was arrested kinetically, the resulting capsid fragments would be well-defined and reminiscent of an incomplete BMV shell, that is, a structure that is larger than the critical nucleus for growth and hence ready to elongate correctly and rapidly if non-cognated RNA is exchanged by cognate RNA. Indeed, there is *in vivo* experimental evidence for small, cellular tRNA-like fragments acting as assembly nuclei and/or chaperoning correct capsid formation when protein concentration is high and could lead to

non-productive aggregation.^[44] However, these fragments efficiently replaced by viral RNA containing both a tRNA-like motif and a specific cis-acting packaging motif in the nonstructural part of the genome.^[45] Thus, the stoichiometric and structural analysis of stressed sub-native cages encapsulating oligonucleotides presented in this report, suggests a tentative mechanism that supports the chaperoning effect of small RNAs while explaining their exclusion from the final assembly result.

It is interesting to note that the occurrence of subviral particles in vivo has been observed for other viruses. For instance, hepatitis B virus-replicating cells can secrete large amounts of spherical (22-nm particles) and filamentous subviral particles consisting only of surface proteins and lacking any capsid and genome.^[46] Although the exact biological role of such particles is still unknown, depending on the ratio of infectious virions to subviral particles, and the time point of addition of subviral particles, viral replication and gene expression can be strongly enhanced or reduced.^[47]

3. Experimental Section

Materials: Ammonium acetate (99.99% trace metals basis), glacial acetic acid, Trizma base (99.9%), cesium chloride (98%), and magnesium acetate tetrahydrate (99%) were purchased from Sigma-Aldrich and used as received. Potassium chloride (99%), sodium citrate dehydrate (99%), and sodium chloride (99%) were purchased from Mallinckrodt chemicals and used as received. Magnesium chloride 6-hydrate (99%) was purchased from J.T. Baker and used as received. Sodium acetate anhydrous (99%) was from EMD and used as received. The 52nt ssDNA oligomers (PolyA and OligoBMV) used were ordered from Invitrogen and were used as received. OligoBMV sequence: 5'-ATGCGGGTACCGTACAGTGTGAAAAACACTGTAAATCTCTAAAAGAGACCA-3'.

Preparation of BMV Capsid Protein: BMV was expressed via the agrobacterium-mediated gene delivery method in *Nicotiana benthamiana*. Plants were allowed to grow for 7 days post infection. The leaves were then collected and homogenized in virus buffer (0.25 M NaOAc, 0.01 M MgCl₂, pH 4.5). The slurry was then centrifuged on a Beckman TA-10.250 rotor at 5000 rpm for 25 min. The supernatant was then centrifuged on a Beckman SW32 rotor for 3 h at 26 000 rpm on a 10% sucrose cushion. The pellet was resuspended in 38.5% CsCl and the virus band was isolated by centrifugation for 24 h on a Beckman TI-71 rotor at 45 000 rpm. The band was dialyzed against SAMA buffer (0.05 M NaOAc, 0.008 M Mg(OAc)₂, pH 4.5), with three changes. The virus was further purified by FPLC equipped with a Superose-6 column. The virus was disassembled and RNA precipitated by dialysis against disassembly buffer (0.5 M CaCl₂, pH 7.4), with three changes of the buffer. RNA was removed by centrifugation on a Beckman TLA 110 rotor at 35 000 rpm for 30 min. The supernatant protein dimers were dialyzed against Tris (0.01 M Tris, pH 7.4) buffer and then TNKM (0.05 M Tris, 0.05 M NaCl, 0.01 M KCl, 0.005 M MgCl₂, pH 7.4) for 24 h each.

Assembly Conditions and Reagents: The protein concentration was kept constant at 0.3 μM for all reactions. The oligomer concentration was varied to produce the varying molar ratios of coat protein to oligomer. Reagents were mixed in 100 mM ammonium acetate (Sigma) that was pH adjusted to 4.5 with acetic acid. Assembly reactions were allowed to proceed for either 1 h or for 2 weeks. At the long reaction time conditions, the assembly reaction is expected to be completed.

CDMS Measurements: The instrument and data analysis methods have been described previously.^[48,49] Briefly, ions are generated by a commercial nanoelectrospray source (TriVersa Nanomate, Advion, Ithaca, NY) and enter the instrument through a heated metal capillary. The ions are separated from the ambient gas flow by several stages of differential pumping that incorporate an ion funnel, an RF hexapole,

and an RF quadrupole. The DC bias on the hexapole (100 V) sets the nominal ion energy. Ions that exit the quadrupole are focused into a dual hemispherical deflection energy analyzer where ions with a narrow band of kinetic energies centered on 100 eV z⁻¹ are selected. The ions are then focused into an electrostatic linear ion trap. Trapped ions oscillate back and forth through a central detection cylinder. When an ion enters the detection cylinder, it induces a charge that is detected by a charge sensitive amplifier. The resulting signal is digitized and transferred to a computer where it is analyzed in real time by fast Fourier transforms (FFTs). The oscillation frequency yields the *m/z* and the FFT magnitude is proportional to the charge. Ions are trapped for 100 ms. Trapping events where ions are not trapped for the full period are discarded. The uncertainty in the charge measurement (which depends on the trapping time) is around 1.1 elementary charges.

Cryo-EM and 3D Reconstruction: To prepare cryo-EM specimen, 4 μL of sample solution was applied on a glow-discharged continuous carbon film coated copper grid (EMS). The grid was frozen using an FEI Vitrobot (Mark III and Mark IV) with the following settings: 25 s wait time, 4 s blotting time, and 100% humidity in Mark III or 15 s blotting time, 0 blotting force, and 100% humidity in Mark IV. Frozen hydrated cryo-EM grids were then transferred 300-kV Titan Krios G3i for BMV-VLP/oligoB or 200-kV Talos Arctica (Thermo Fisher Scientific) for BMV-VLP/polyA. Data collection utilized EPU automation software under low dose setup where images were acquired on a Gatan K3 (for VLP/oligoB) or a TFS Falcon III (for VLP/PolyA) direct electron detector using electron counting mode. For each image, a total dose of 30 e-Å⁻² was used with frame dose rate at 1 e-Å⁻². The effective pixel size for both data is 0.84 Å. Particle picking was done semi-manually using e2boxer.py in EMAN2 (v2.23).^[50] Motion correction, 2D classification, initial model building, and 3D refinement were performed using Relion (v3.0.8).^[51] Focus refinement was performed using the protocol established earlier.^[52,53] The estimated final resolution for each structure is 3.6 Å (BMV-VLPH8/oligoB), 4.3 Å (BMV-VLPH15/oligoB), 5.3 Å (BMV-VLPH8/polyA), and 7.2 Å (BMV-VLPH15/polyA). The 3D structures were visualized using UCSF Chimera^[54] and ChimeraX.^[55] Data processing statistics are given in Table S1, Supporting Information.

Supporting Information

Supporting Information is available from the Wiley Online Library or from the author.

Acknowledgements

The work was supported by the Army Research Office, under award W911NF-17-1-0329, the National Science Foundation, under award CBET 1803440, and by the NIH under award number 1RO1AI118933. The authors gratefully acknowledge Indiana University at Bloomington for access to the Electron Microscopy Center and the Nanoscience Characterization Facility and the Pennsylvania State University College of Medicine for access to the Thermo Scientific Titan Krios.

Conflict of Interest

The authors declare no conflict of interest.

Keywords

brome mosaic virus, charge detection mass spectrometry, cryo-electron microscopy, virus assembly

Received: July 24, 2020

Revised: October 21, 2020

Published online: November 25, 2020

- [1] P. E. Prevelige Jr., *J. Mol. Biol.* **2011**, *410*, 634.
- [2] L. Ruan, J. A. Hadden, A. Zlotnick, *J. Virol.* **2018**, *92*, 20.
- [3] T. Douglas, M. Young, *Science* **2006**, *312*, 873.
- [4] B. Dragnea, *ACS Nano* **2017**, *11*, 3433.
- [5] J. D. Perlmutter, M. F. Hagan, *Annu. Rev. Phys. Chem.* **2015**, *66*, 217.
- [6] S. E. Aniagyei, C. DuFort, C. C. Kao, B. Dragnea, *J. Mater. Chem.* **2008**, *18*, 3763.
- [7] M. Comas-Garcia, *Viruses* **2019**, *11*, 3.
- [8] V. A. Belyi, M. Muthukumar, *Proc. Natl. Acad. Sci.* **2006**, *103*, 17174.
- [9] R. F. Garmann, M. Comas-Garcia, M. S. T. Koay, J. J. L. M. Cornelissen, C. M. Knobler, W. M. Gelbart, *J. Virol.* **2014**, *88*, 10472.
- [10] R. Zandi, B. Dragnea, A. Travesset, R. Podgornik, *Phys. Rep.* **2020**, *847*, 1.
- [11] R. Twarock, P. G. Stockley, *Annu. Rev. Biophys.* **2019**, *48*, 495.
- [12] N. Patel, S. J. White, R. F. Thompson, R. Bingham, E. U. Weiß, D. P. Maskell, A. Zlotnick, E. C. Dykeman, R. Tuma, R. Twarock, N. A. Ranson, P. G. Stockley, *Nat. Microbiol.* **2017**, *2*, 17098.
- [13] E. C. Dykeman, P. G. Stockley, R. Twarock, *Proc. Nat. Acad. Sci. USA* **2014**, *111*, 5361.
- [14] Y. G. Choi, G. L. Grantham, A. L. Rao, *Virology* **2000**, *270*, 377.
- [15] Y. G. Choi, A. L. Rao, *Virology* **2000**, *275*, 207.
- [16] C. Chen, J. C. Wang, E. E. Pierson, D. Z. Keifer, M. Delaleau, L. Gallucci, C. Cazenave, M. Kann, M. F. Jarrold, A. Zlotnick, *PLoS Pathog.* **2016**, *12*, e1005802.
- [17] D. Z. Keifer, D. L. Shinholt, M. F. Jarrold, *Anal. Chem.* **2015**, *87*, 10330.
- [18] M. A. Krol, N. H. Olson, J. Tate, J. E. Johnson, T. S. Baker, P. Ahlquist, *Proc. Natl. Acad. Sci.* **1999**, *96*, 13650.
- [19] S. J. Maassen, M. V. de Ruyter, S. Lindhoud, J. J. L. M. Cornelissen, *Chem. Eur. J.* **2018**, *24*, 7456.
- [20] A. R. Thurm, C. Beren, A. L. Duran-Meza, C. M. Knobler, W. M. Gelbart, *Biophys. J.* **2019**, *117*, 1331.
- [21] A. Rao, G. L. Grantham, *Virology* **1996**, *226*, 294.
- [22] P. Ni, Z. Wang, X. Ma, N. C. Das, P. Sokol, W. Chiu, B. Dragnea, M. Hagan, C. C. Kao, *J. Mol. Biol.* **2012**, *419*, 284.
- [23] R. D. Cadena-Nava, M. Comas-Garcia, R. F. Garmann, A. L. N. Rao, C. M. Knobler, W. M. Gelbart, *J. Virol.* **2012**, *86*, 3318.
- [24] C. Beren, L. L. Dreesens, K. N. Liu, C. M. Knobler, W. M. Gelbart, *Biophys. J.* **2017**, *113*, 339.
- [25] H. G. Hansma, I. Revenko, K. Kim, D. E. Laney, *Nucleic Acids Res.* **1996**, *24*, 713.
- [26] C. J. Schlicksup, J. C.-Y. Wang, S. Francis, B. Venkatakrishnan, W. W. Turner, M. VanNieuwenhze, A. Zlotnick, *eLife* **2018**, *7*, e31473.
- [27] J. C. Y. Wang, C. Chen, V. Rayaprolu, S. Mukhopadhyay, A. Zlotnick, *ACS Nano* **2015**, *9*, 8898.
- [28] E. E. Pierson, D. Z. Keifer, A. A. Kukreja, J. C.-Y. Wang, A. Zlotnick, M. F. Jarrold, *J. Mol. Biol.* **2016**, *428*, 292.
- [29] J. Tang, J. M. Johnson, K. A. Dryden, M. J. Young, A. Zlotnick, J. E. Johnson, *J. Struct. Biol.* **2006**, *154*, 59.
- [30] J. Zivanov, T. Nakane, B. O. Forsberg, D. Kimanius, W. J. H. Hagen, E. Lindahl, S. H. W. Scheres, *Elife* **2018**, *7*, e2166.
- [31] G. Vigers, R. Crowther, B. Pearse, *EMBO J.* **1986**, *5*, 529.
- [32] A. Fotin, T. Kirchhausen, N. Grigorieff, S. C. Harrison, T. Walz, Y. F. Cheng, *J. Struct. Biol.* **2006**, *156*, 453.
- [33] A. Zlotnick, *J. Mol. Biol.* **1994**, *241*, 59.
- [34] D. C. Rapaport, *Phys. Rev. E* **2004**, *70*, 13.
- [35] M. F. Hagan, D. Chandler, *Biophys. J.* **2006**, *91*, 42.
- [36] H. D. Nguyen, V. S. Reddy, C. L. Brooks, *Nano Lett.* **2007**, *7*, 338.
- [37] R. F. Bruinsma, M. Comas-Garcia, R. F. Garmann, A. Y. Grosberg, *Phys. Rev. E* **2016**, *93*, 032405.
- [38] J. Wagner, R. Zandi, *Biophys. J.* **2015**, *109*, 956.
- [39] S. Panahandeh, S. Li, R. Zandi, *Nanoscale* **2018**, *10*, 22802.
- [40] M. J. Bowick, D. R. Nelson, H. Shin, *Phys. Chem. Chem. Phys.* **2007**, *9*, 6304.
- [41] A. Luque, D. Reguera, A. Morozov, J. Rudnick, R. Bruinsma, *J. Chem. Phys.* **2012**, *136*, 184507.
- [42] S. Panahandeh, S. Li, L. Marichal, R. Leite Rubim, G. Tresset, R. Zandi, *ACS Nano* **2020**, *14*, 3170.
- [43] M. J. Bowick, L. Giomi, *Adv. Phys.* **2009**, *58*, 449.
- [44] Y. G. Choi, T. W. Dreher, A. L. N. Rao, *Proc. Natl. Acad. Sci.* **2002**, *99*, 655.
- [45] Y. G. Choi, A. L. N. Rao, *J. Virol.* **2003**, *77*, 9750.
- [46] N. Chai, H. Chang, E. Nicolas, Z. Han, M. Jarnik, J. Taylor, *J. Virol.* **2008**, *82*, 7812.
- [47] M. Bruns, S. Miska, S. Chassot, H. Will, *J. Virol.* **1998**, *72*, 1462.
- [48] N. C. Contino, M. F. Jarrold, *Int. J. Mass Spectrom.* **2013**, *345–347*, 153.
- [49] N. C. Contino, E. E. Pierson, D. Z. Keifer, M. F. Jarrold, *J. Am. Soc. Mass Spectrom.* **2013**, *24*, 101.
- [50] S. J. Ludtke, *Methods Enzymol.* **2016**, *579*, 159.
- [51] S. H. Scheres, *Methods Enzymol.* **2016**, *579*, 125.
- [52] S. L. Ilca, A. Kotecha, X. Sun, M. M. Poranen, D. I. Stuart, J. T. Huiskonen, *Nat. Commun.* **2015**, *6*, 8843.
- [53] C. J. Schlicksup, P. Laughlin, S. Dunkelbarger, J. C.-Y. Wang, A. Zlotnick, *ACS Chem. Biol.* **2020**, *15*, 1708.
- [54] E. F. Pettersen, T. D. Goddard, C. C. Huang, G. S. Couch, D. M. Greenblatt, E. C. Meng, T. E. Ferrin, *J. Comput. Chem.* **2004**, *25*, 1605.
- [55] T. D. Goddard, C. C. Huang, E. C. Meng, E. F. Pettersen, G. S. Couch, J. H. Morris, T. E. Ferrin, *Protein Sci.* **2018**, *27*, 14.